Cell Reports
Article



# Alternative Spliceosome Assembly Pathways Revealed by Single-Molecule Fluorescence Microscopy

Inna Shcherbakova,[1,2] Aaron A. Hoskins,[1,2,4] Larry J. Friedman,[2] Victor Serebrov,[1,2] Ivan R. Corrêa, Jr.,[3] Ming-Qun Xu,[3] Jeff Gelles,[2,*] and Melissa J. Moore[1,*]
[1]Department of Biochemistry and Molecular Pharmacology, Howard Hughes Medical Institute, University of Massachusetts Medical School, Worcester, MA 01605, USA
[2]Department of Biochemistry, Brandeis University, Waltham, MA 02454, USA
[3]New England Biolabs, Ipswich, MA 01938, USA
[4]Present address: Department of Biochemistry, University of Wisconsin-Madison, Madison, WI 53706, USA
*Correspondence: gelles@brandeis.edu (J.G.), melissa.moore@umassmed.edu (M.J.M.)
http://dx.doi.org/10.1016/j.celrep.2013.08.026


## SUMMARY

**Removal of introns from nascent transcripts (pre-mRNAs) by the spliceosome is an essential step in eukaryotic gene expression. Previous studies have suggested that the earliest steps in spliceosome assembly in yeast are highly ordered and the stable recruitment of U1 small nuclear ribonucleoprotein particle (snRNP) to the 5′ splice site necessarily precedes recruitment of U2 snRNP to the branch site to form the "prespliceosome." Here, using colocalization single-molecule spectroscopy to follow initial spliceosome assembly on eight different *S. cerevisiae* pre-mRNAs, we demonstrate that active yeast spliceosomes can form by both U1-first and U2-first pathways. Both assembly pathways yield prespliceosomes functionally equivalent for subsequent U5·U4/U6 tri-snRNP recruitment and for intron excision. Although fractional flux through the two pathways varies on different introns, both are operational on all introns studied. Thus, multiple pathways exist for assembling functional spliceosomes. These observations provide insight into the mechanisms of cross-intron coordination of initial spliceosome assembly.**

## INTRODUCTION

Excision of introns from precursors to messenger RNAs (pre-mRNA splicing) is carried out by the spliceosome, a multimegadalton machine composed of five small nuclear ribonucleoprotein particles (snRNPs) (U1, U2, U4, U5, and U6 snRNPs), the protein-only Prp19 complex (NTC), and numerous transiently interacting splicing factors. For each round of intron excision, these pieces must assemble into an active spliceosome. Ensemble studies following the appearance and disappearance of stable complexes in vitro (Ruby and Abelson, 1988; Seraphin and Rosbash, 1989) and the accumulation of chromatin IP (ChIP) signatures for snRNPs in vivo (Görnemann et al., 2005; Moore et al., 2006; Tardiff et al., 2006) have led to a widely accepted model for early spliceosome assembly across yeast introns wherein 5′ splice site (SS) recognition by U1 precedes branch site (BS) recognition by U2 (reviewed in Hoskins and Moore, [2012], Matlin and Moore [2007], Staley and Woolford [2009], and Wahl et al. [2009]). After establishment of a U1·U2 prespliceosome (A complex), U5·U4/U6 tri-snRNP addition (to form B complex) is quickly followed by NTC acquisition and subsequent structural rearrangements, culminating in a catalytically active spliceosome (C complex; Figure 1A). Using colocalization single-molecule spectroscopy (CoSMoS) (Friedman et al., 2006) to directly observe the real-time dynamics of subcomplex associations with surface-tethered pre-mRNA molecules in *S. cerevisiae* whole cell extract (WCE) (Crawford et al., 2008), we recently confirmed that spliceosome assembly on *RP51A* pre-mRNA, an optimized splicing substrate containing a shortened intron (Pikielny et al., 1986), occurs predominantly by this ordered U1 → U2 → U5·U4/U6 → NTC pathway (Hoskins et al., 2011).

Is this single highly ordered assembly pathway the same for all yeast introns? To address this, we here selected for CoSMoS seven additional single-intron pre-mRNAs from *S. cerevisiae.* In ensemble splicing assays, these pre-mRNAs displayed a wide range of splicing rates and efficiencies. We then examined the rates and binding order for all major subcomplexes via CoSMoS. This revealed an alternate spliceosome assembly pathway, wherein U2 is recruited before U1. Both the U1-first and U2-first pathways were used on all pre-mRNAs studied, including *RP51A*, but the fractional fluxes through these pathways varied widely for different pre-mRNAs. Additional experiments revealed that U1·U2·pre-mRNA prespliceosomal complexes formed by either the U1-first or U2-first pathway are functionally equivalent for both tri-snRNP recruitment and intron excision. Taken together, our results show that there is no requisite binding order for U1 and U2 during the initial stage of spliceosome assembly. Both the high reversibility of U1

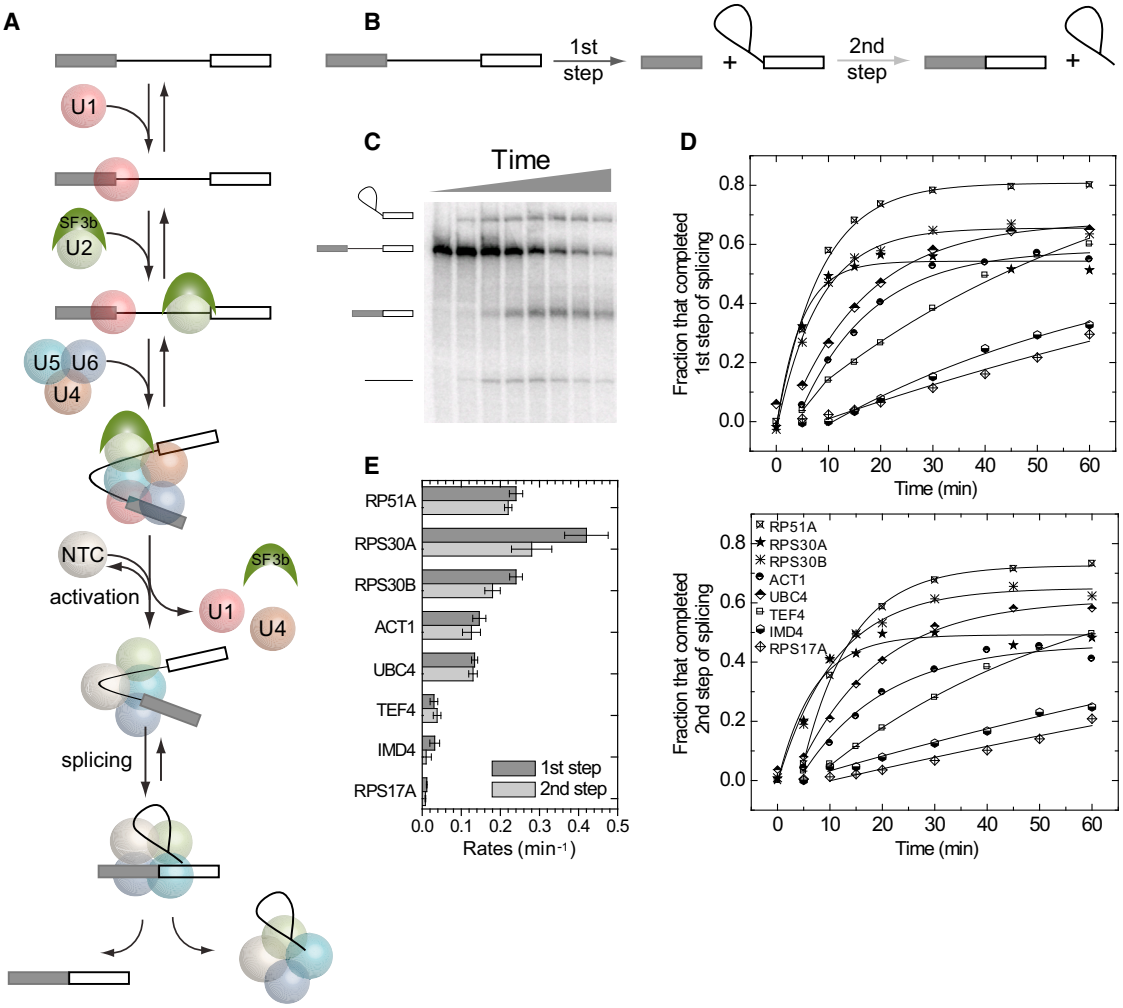


**Figure 1. Splicing of *S. cerevisiae* Pre-mRNAs Studied in Ensemble Experiments In Vitro**

(A) Spliceosome assembly and splicing pathway for *RP51A* pre-mRNA (Hoskins et al., 2011). Rectangles, exons; line, intron.

(B) Cartoon showing the first and second chemical steps of splicing.

(C) Products of the first and second step reactions of radioactively labeled *RP51A* pre-mRNA incubated with WCE in the presence of ATP for 0–60 min and visualized by denaturing PAGE.

(D) Fraction of molecules that completed the first and second steps of splicing for eight different pre-mRNAs as a function of incubation time.

(E) Compiled first (darker bars) and second step (lighter bars) rates (±SE) for the specified pre-mRNAs.

binding and the existence of multiple alternative assembly pathways have implications for our understanding of the cross-intron coordination of initial spliceosome assembly in vivo and of regulated splice site pairing that closely follows prespliceosome formation in higher eukaryotes (Kotlajich et al., 2009).

## RESULTS

### Ensemble Splicing Rates and Efficiencies Differ for Different Pre-mRNAs

Very few *S. cerevisiae* pre-mRNAs have previously been analyzed in in vitro splicing reactions. To remedy this, we selected eight single-intron pre-mRNAs with diverse features (Table 1). Included were both *RP51A*, the optimized splicing substrate (Pikielny et al., 1986) we used in our previous CoSMoS study (Hoskins et al., 2011), and the full-length intron from its parent gene (RPS17A). *ACT1* and *UBC4* are two other well-studied introns (Abelson et al., 2010; Ruby and Abelson, 1988). The introns of *TEF4* and *IMD4* contain snoRNAs, so are likely highly structured (Villa et al., 2000). *RPS30A* and *RPS30B*, which both encode the same ribosomal protein, displayed differential sensitivities to mutations in core spliceosome components in vivo (Pleiss et al., 2007); this suggested that splicing of these two introns might be governed by different rate-limiting steps.

*RP51A* pre-mRNA was generated as previously described (Hoskins et al., 2011). For the seven endogenous introns, pre-mRNAs were transcribed from PCR products amplified from genomic DNA of strain BJ2168. Because *S. cerevisae* introns tend to be located very close to the transcription start site (Fink, 1987), each in vitro-transcribed pre-mRNA consisted of

**Table 1. Pre-mRNAs Examined in This Study**

| Name | Features | Schematic | 5'SS | BS | 3'SS |
|---|---|---|---|---|---|
| RP51A | Model pre-mRNA with shortened intron | 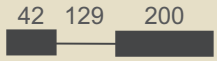  | GUAUGU | UACUAAC | UAG |
| RPS30A | Differentially affected by mutations in core spliceosome components |   | GUACGU | UACUAAC | UAG |
| RPS30B | | 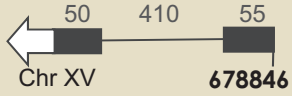  | GUACGU | UACUAAC | UAG |
| ACT1 | Full length parent of well-studied model pre-mRNA |   | GUAUGU | UACUAAC | UAG |
| UBC4 | Model pre-mRNA with a short intron | 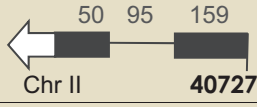  | GUAUGU | UACUAAC | UAG |
| TEF4 | snoRNA (snR38) in intron | 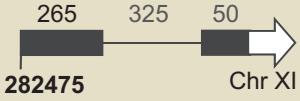  | GUAUGU | UACUAAC | UAG |
| IMD4 | snoRNA (snR45) in intron | 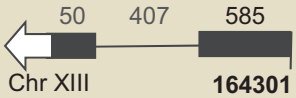  | GUAUGU | UACUAAC | CAG |
| RPS17A | Full-length parent of RP51A | 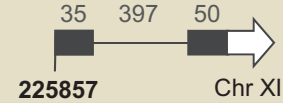  | GUAUGU | UACUAAC | UAG |

Schematics indicate exons (blocks), introns (lines), and their lengths in nucleotides (numbers above). Except for *RP51A*, each pre-mRNA began at the 5′ end of the endogenous transcript (chromosomal position indicated below; Xu et al., 2009). Right and left arrows indicate Watson and Crick transcripts. Underlined letters in the 5′ splice site (SS) sequence column indicate deviations from the canonical sequences.

the entire first exon, the intron, and 50 nucleotides of the second exon of the parent gene. When assayed in bulk splicing reactions, first and second step products could be observed for all eight pre-mRNA species. Thus, the ability to splice in vitro seems to be a general feature of yeast introns. Nonetheless, they exhibited significantly different rates and yields for the two chemical steps of splicing (Figure 1). The difference in splicing rates between the fastest and slowest pre-mRNAs, *RPS30A* and *RPS17A*, respectively, was >30-fold.

### Subcomplex Association Kinetics Are Similar for Pre-mRNAs that Are Spliced at Widely Different Rates

To determine if the above ensemble splicing rate differences (Figure 1E) were attributable to different rates of subcomplex association, we employed CoSMoS experiments to individually monitor U1, U2, U5, and NTC binding dynamics on all eight pre-mRNA species. These experiments were performed in WCEs, in which the subcomplex of interest was fluorescently labeled by a tight, noncovalent interaction between two protein substituents carrying a C-terminal *E. coli* dihydrofolate reductase (eDHFR) tag and a trimethoprim-dye conjugate. We exposed surface-tethered, dye labeled pre-mRNA molecules to WCE (Figure 2A). Subcomplex binding was detected as colocalization of subcomplex and pre-mRNA fluorescent labels (Figure 2B). Neither photobleaching (see Experimental Procedures) nor dye exchange (Hoskins et al., 2011) contributes significantly to the subcomplex dynamics observed under the experimental conditions used here. Control samples lacking surface-tethered pre-mRNAs exhibited very few binding events for any of the four subcomplexes. For each pre-mRNA species, hundreds of individual molecules were analyzed (n = 153 to 422), allowing production of rastergrams (digital representations of single-molecule fluorescence time records) that display the binding dynamics of each subcomplex (Figures 2C and 2D).

In these experiments, the majority of pre-mRNA molecules bound each subcomplex at least once. Further, as observed in previous work on *RP51A* (Hoskins et al., 2011), many pre-mRNA molecules bound a given subcomplex multiple times (Figure S1A). Thus reversible binding of individual subcomplexes is a common feature of initial spliceosome assembly on many pre-mRNAs. As we previously reported, U1 snRNP exhibited the most dynamic binding (during the first 20 min, an average of 3.2 ± 0.5 [SEM] binding events lasting ≥1.5 s were observed per pre-mRNA molecule), with the other subcomplexes being

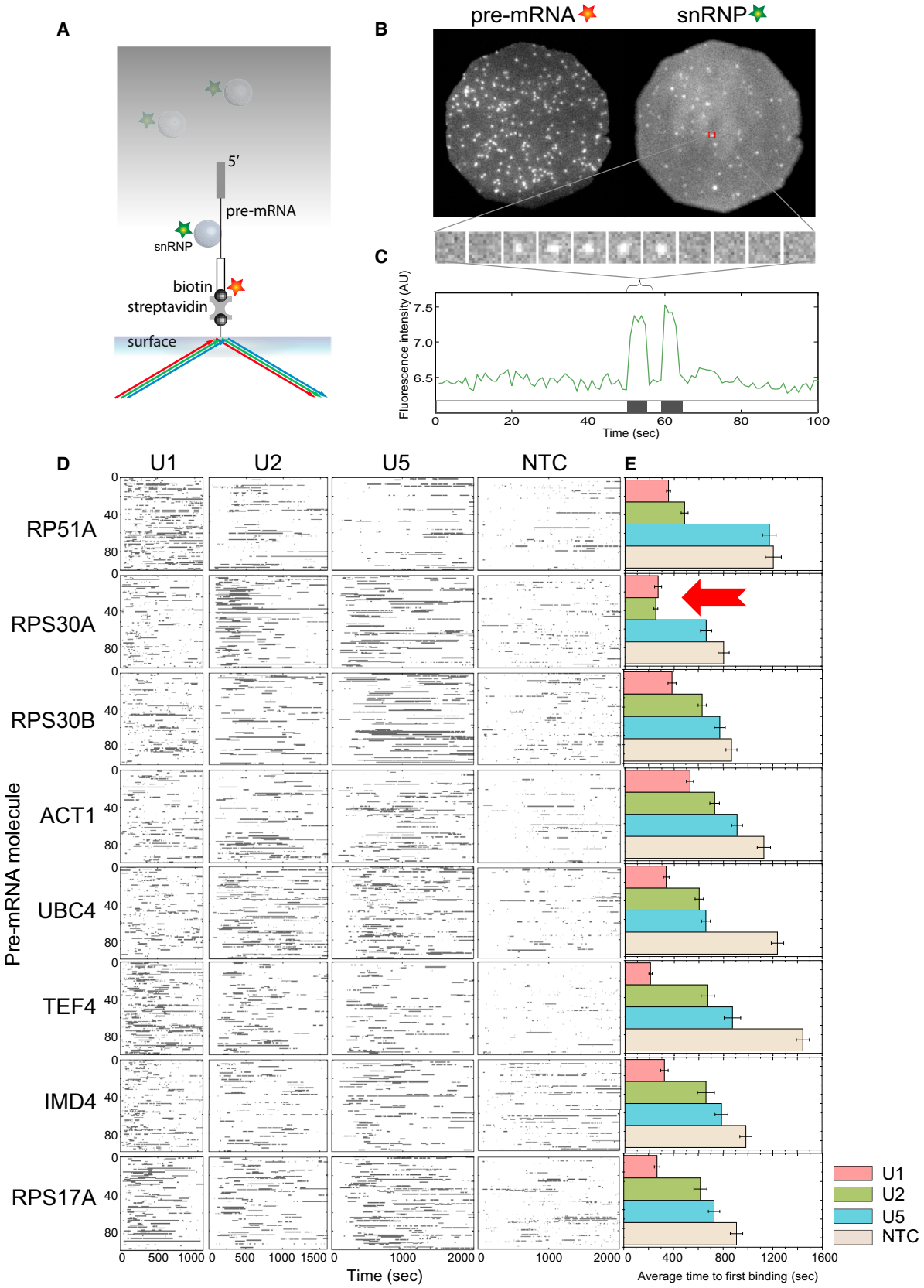


*(legend on next page)*

less dynamic (1.7 ± 0.2 for U2; 1.9 ± 0.3 for U5; 1.4 ± 0.2 for NTC). Among pre-mRNA species, there was no apparent correlation between the splicing rate (Figures 1D and 1E) and either the percentage of pre-mRNA molecules that bound individual subcomplexes or the total number of subcomplex binding events (Figure S1A). Therefore, the >30-fold range in splicing rates cannot be readily explained by differences in subcomplex binding rates or the apparent ratio between productive and unproductive events.

In addition to the number of binding events, our single-molecule traces allowed us to examine the kinetics of subcomplex association. We observed that different pre-mRNA species exhibited distinct kinetics. For example, much of the U2 association with *RPS30A* occurred in the first 500 s, whereas U2 association with *UBC4* was more uniformly distributed across the 1,600 s time course shown (Figure 2D). Nevertheless, when the subcomplex binding data are considered as a whole (Figure 2E), there is no single subcomplex binding step whose kinetics appear to explain the >30-fold range in splicing rates (Figure 1). Notably, even the most poorly spliced pre-mRNAs in our set (*TEF4*, *IMD4*, and *RPS17A*) displayed average times to first subcomplex binding that were similar to (or at most 2-fold greater than) those of the fastest splicing pre-mRNAs. Further, for all three species, >48% of pre-mRNA molecules exhibited one or more long-lived (≥1.5 s) U5 binding events and >33% exhibited one or more long-lived NTC binding events during the first 20 min of the experiment (Figure S1A). Thus, we hypothesize that the low splicing efficiencies for *TEF4*, *IMD4*, and *RPS17A* are not due to their failure to enter and proceed along the initial spliceosome assembly pathway.

Taken together, the data characterizing subcomplex recruitment by (Figure 2) and splicing rates and efficiencies for different pre-mRNAs demonstrate that processes other than subcomplex binding kinetics must account for the differences in splicing rates observed *in vitro*. A likely explanation is that different rates of activation or chemistry after the spliceosome is assembled account for the broad range of splicing kinetics observed.

## U1·U2·pre-mRNA Prespliceosome Formation prior to Tri-snRNP Recruitment Is a General Feature of Yeast Spliceosome Assembly

In our previous CoSMoS study (Hoskins et al., 2011), we used dual-labeled WCEs to examine the order in which spliceosomal subcomplexes bound to pre-mRNA molecules. This analysis revealed that, for *RP51A* pre-mRNA, U1 generally binds before U2 and U2 generally binds before the U5·U4/U6 tri-snRNP. However, those experiments were unable to reveal whether tri-snRNP binding requires prior formation of an U1·U2·pre-mRNA complex, as suggested by the sequential spliceosome assembly model (Figure 1A). To test whether U1·U2·pre-mRNA complex formation generally precedes tri-snRNP recruitment, we performed CoSMoS experiments with triply labeled WCE, in which U1, U2, and U5 were each labeled with a different colored fluorophore. For these experiments, we used *RP51A*, *RPS30A*, *RPS30B*, *ACT1*, *UBC4*, and *RPS17A* pre-mRNAs.

Pre-mRNA molecules were first attached to the surface and the surface density verified by imaging a dye label on the RNA. This dye was then photobleached to avoid interference with subsequent subcomplex imaging. Next, we introduced the triply labeled WCE (Figure 3A). Control samples lacking surface-tethered pre-mRNAs exhibited very few binding events for any of the three subcomplexes (Figure S2C). In contrast, when a pre-mRNA was present, fluorescent spots of each of the three colors were readily observable (Figure 3B and S2A) and often occurred either simultaneously or sequentially at the same position in the microscope field. Given the low pre-mRNA surface densities used, these colocalized spots likely represented subcomplexes binding to a single pre-mRNA molecule. Consistent with earlier studies (Ruby and Abelson, 1988), only U1 accumulation was observed in the absence of ATP (Figure S2B).

To assess whether U5·U4/U6 tri-snRNP binding requires prior formation of a U1·U2·pre-mRNA prespliceosome, we first picked pre-mRNA molecules that displayed U5 binding events. For each of the six pre-mRNA species examined, 90%–95% of the U5 binding events were preceded by the observed simultaneous presence of U1 and U2 on the same pre-mRNA molecule (n = 521 to 651 for each pre-mRNA species). This high degree of correlation suggests that tri-snRNP binding requires prior U1·U2·pre-mRNA prespliceosome formation. To exclude the possibility that this apparent correlation resulted simply from the faster binding kinetics of U1 and U2 compared to U5, we performed a control analysis in which we examined whether each U5 binding event on a pre-mRNA molecule was preceded by U1·U2·pre-mRNA prespliceosome formation on a different, randomly chosen pre-mRNA. For *RPS30A* (which is the most stringent test, because it displayed the fastest U2 binding kinetics; Figure 2E), the correlation measured in the control analysis, 65% ± 3% (n = 286) was significantly lower than the

**Figure 2. Recruitment of Individual Spliceosomal Subcomplexes to Single Surface-Tethered Pre-mRNA Molecules Observed by CoSMoS**

(A) Experimental design. Spliceosomal subcomplexes (circles) labeled with a green dye (star) colocalized with surface-tethered pre-mRNA molecules labeled with a red dye (star) were visualized by total internal reflection fluorescence (TIRF) microscopy using excitation with red and green lasers (arrows). Subcomplexes free in bulk solution (gray shading) were not detected.

(B) Example CoSMoS data showing binding of U1 snRNP to *ACT1* pre-mRNA. Fluorescence emission from a single field of view (diameter 24 μm) was separated to produce images of pre-mRNA and U1 snRNP molecules. Individual molecules are detected as discrete spots of fluorescence; red squares mark an example of a pre-mRNA molecule with U1 bound.

(C) Top: part of the time series of U1 fluorescence images taken from the location of the pre-mRNA molecule marked in (B) (1 s per frame). Bottom: complete time record of U1 fluorescence from the same pre-mRNA. Intervals in which U1 is colocalized with the pre-mRNA are indicated as black bands on the time ribbon.

(D) Rastergrams (stacked time ribbons for multiple individual pre-mRNA molecules) summarizing the recruitment of the U1, U2, U5, and NTC by eight different pre-mRNAs. Each rastergram shows data on 100 pre-mRNA molecules taken from a separate experiment (32 experiments total). Only the first 1,100, 1,600, 2,000, and 2,000 s of data are shown for U1, U2, U5, and NTC, respectively.

(E) Average time (±SEM) to first binding of the indicated subcomplex to each pre-mRNA molecule.

See also Figure S1.

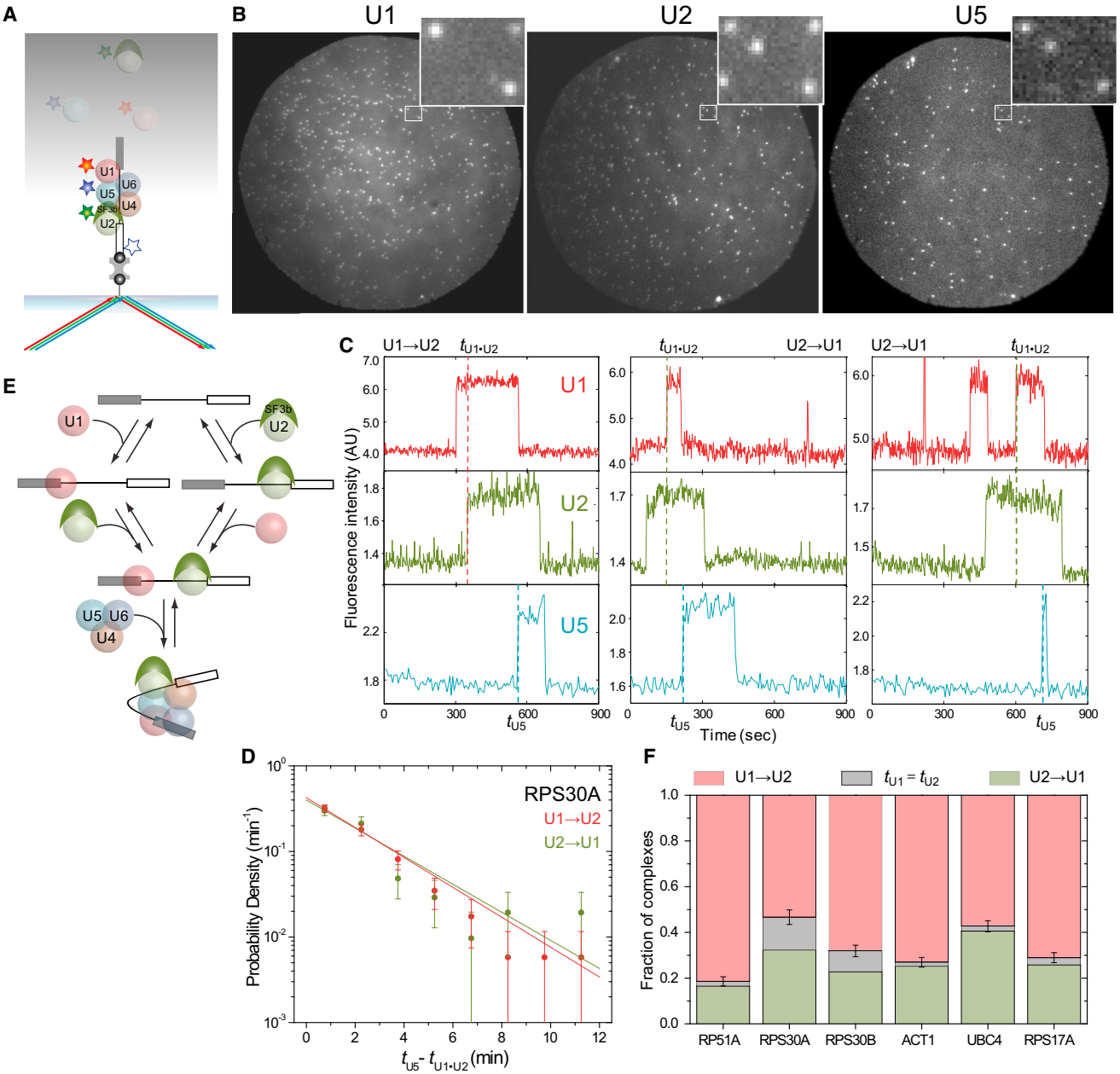


**Figure 3. Sequence of U1, U2, and U5 Binding to Surface-Tethered Pre-mRNAs**

(A) Experimental design. Surface-tethered pre-mRNA was labeled with a blue fluorophore that was used to monitor pre-mRNA surface density. Before the experiment, this fluorophore was photobleached (white star with blue outline) so as not to interfere with detection of U5 fluorescence. U1, U2, and U5 in WCE were each dye labeled; binding to the pre-mRNA was detected with red, green, and blue lasers, respectively. Only events in which formation of a U1•U2•pre-mRNA prespliceosome was followed by U5 binding were selected for analysis.

(B) Example images. Fluorescence of U1 (left), U2 (center), and U5 (right) was recorded from a single field of view at 1,110 s after addition of triple-labeled WCE containing ATP to a chamber with surface-immobilized *UBC4* pre-mRNA. Insets show magnified images from the same 3.54 × 2.93 μm area of the chamber surface (white frames).

(C) Example segments of fluorescence records of U1, U2, and U5 binding to three *RPS30A* pre-mRNA molecules. Prespliceosome formation by the U1 → U2 (red dashed line) and U2 → U1 (green dashed line) pathways is marked.

(D) Distribution (±SE) of the time intervals ($t_{U5} - t_{U1•U2}$) between the formation of the U1•U2•*RPS30A* pre-mRNA complex and the binding of U5. Prespliceosomes that formed by the U1 → U2 (red) and U2 → U1 (green) pathways were analyzed separately; exponential fits (lines) yielded apparent first-order rate constants for U5 binding to the U1•U2•pre-mRNA complex of 0.40 ± 0.05 and 0.36 ± 0.06 min$^{-1}$, respectively.

(E) Summary of the pathways observed in this experiment. Spliceosome assembly up to B complex (bottom) can occur via both U1 → U2 and U2 → U1 branches.

(F) Fraction (±SE) of complexes that formed through the U1 → U2 (red) or U2 → U1 (green) pathways or for which the pathway was indeterminate (gray).

See also Figure S2.

same molecule measurement 93% ± 1% (n = 488; p = $10^{-20}$, assuming the errors are normally distributed). We conclude that, on all introns tested, most or all U5•U4/U6 tri-snRNP binding requires prior U1•U2•pre-mRNA prespliceosomal complex formation. Ordered formation of the prespliceosome and B complex is thus likely to be a general feature of yeast spliceosome assembly.

## Prespliceosomal Complexes on Pathway for Tri-snRNP Addition Can Form by First Recruiting Either U1 or U2

Having confirmed that U1•U2•pre-mRNA prespliceosome formation generally precedes tri-snRNP recruitment on our set of yeast pre-mRNAs, we next investigated whether U1 recruitment must precede U2 in order to recruit the tri-snRNP. Consistent with such a highly ordered U1 → U2 → U5•U4/U6 → NTC assembly pathway (Hoskins et al., 2011), the average time to first binding of a given subcomplex to pre-mRNA occurred in the order U1 < U2 < U5 < NTC on seven of our eight pre-mRNA species (Figure 2E). For *RPS30A*, however, the pattern was U1 ≈ U2 < U5 < NTC (Figure 2E, arrow), suggesting that a significant fraction of *RPS30A* molecules might first bind U2 simultaneously with or prior to U1. Experiments with *RPS30A* in dual-labeled WCE, in which U1 and U2 were labeled with different colored fluorophores, confirmed that ~40% of *RPS30A* pre-mRNA molecules appeared to recruit U2 prior to U1 (Figure S1B). In contrast, U2 bound first to <10% of *RP51A* molecules in our studies. Thus, U1•U2•pre-mRNA complex formation on *RPS30A* pre-mRNA may not be as highly ordered as on *RP51A* pre-mRNA.

Are U1•U2•pre-mRNA complexes formed by the U1-first and U2-first pathways equally competent for U5•U4/U6 tri-snRNP recruitment? Within the triply labeled WCE data set (Figures 3A and 3B), we could readily observe U5 binding to prespliceosomes formed by either the U1-first (Figure 3C, left) or the U2-first pathway (Figure 3C, center and right). To examine the U5 binding rates for *RPS30A* prespliceosomes formed by either pathway, we measured for each U5 binding event $t_{U5} - t_{U1\cdot U2}$, the time between arrival of the final component of the prespliceosome and arrival of U5 (Figure 3C). The distribution of $t_{U5} - t_{U1\cdot U2}$ values was exponential, consistent with a single rate-limiting step between prespliceosome formation and tri-snRNP association, as was previously inferred for *RP51A* pre-mRNA (Hoskins et al., 2011). When we separately considered complexes produced by the U1-first versus U2-first assembly pathways, the $t_{U5} - t_{U1\cdot U2}$ distributions were indistinguishable (Figures 3D and S2D). In addition, the assembly pathway had no effect on the efficiency of tri-snRNP recruitment, with 80% ± 3% of all U1 → U2 complexes and 83% ± 5% of all U2 → U1 prespliceosomes recruiting U5, respectively. Thus, prespliceosomes formed by the two pathways are equally competent to perform the next major step in spliceosome assembly and are likely to be identical (Figure 3E).

## All Pre-mRNAs Exhibit Both U1- and U2-First Pathways

Having found that prespliceosomes capable of recruiting the U5•U4/U6 tri-snRNP could assemble by either a U1-first or U2-first pathway on *RPS30A* pre-mRNA, we next wondered whether this was also true for other pre-mRNAs. Therefore, we analyzed, as for *RPS30A*, the triply labeled WCE data for *RP51A*, *RPS30B*, *ACT1*, *UBC4*, and *RPS17A* pre-mRNAs. Remarkably, this revealed that prespliceosomes capable of recruiting U5 could assemble by either the U1-first or U2-first pathway for all six pre-mRNAs. However, the prevalence of the two pathways differed among pre-mRNA species (Figure 3F). At one extreme was *RP51A*, for which 81% ± 2.1% of molecules went through the U1 → U2 pathway, a result consistent with both previous ensemble data (Seraphin and Rosbash, 1989) and our previous single-molecule observations (Hoskins et al., 2011), given the different data acquisition rates and analytical methods employed (see Experimental Procedures). At the other extreme were *UBC4* and *RPS30A*, for which 43% ± 2.4% to 47% ± 3.4% of molecules, respectively, either recruited U2 before U1 or recruited them simultaneously within the time resolution of the experiment. Thus, the ability to form a prespliceosome functional for tri-snRNP recruitment is not a strictly ordered process for any pre-mRNA studied, but the U1-first and U2-first pathways are used to different extents on different pre-mRNAs.

## Pre-mRNAs that Initiate Spliceosome Assembly via the U1- or U2-First Pathways Are Equally Competent for Splicing

Because the above experiments demonstrated that prespliceosomes formed by the U1-first and U2-first pathways were equally competent for tri-snRNP recruitment, we next asked whether they were also equally competent for splicing. To address this, we synthesized *RPS30A* pre-mRNA containing an average of eight fluorophores within the intron and performed CoSMoS experiments with WCE, in which U1 and U2 were labeled with different colored fluorophores (Figure 4A). For these experiments, U1 and U2 fluorescence was monitored continuously (1 s frames), but the intron fluorescence was monitored only once every 2.5 min to limit photobleaching of the pre-mRNA dyes. Because splicing requires ATP, experiments lacking ATP could be used to determine the extent of intron fluorophore photobleaching. Without ATP, 11% of RNA molecules had completely lost intron fluorescence by the end of 28 min of observation (Figure 4B) and fluorescence loss by single molecules occurred in multiple small steps consistent with successive photobleaching of the dyes (as in Figure 4C, bottom). In the presence of ATP, a much larger fraction of molecules (57%) lost intron fluorescence (Figure 4B), and in many cases, most or all of the fluorescence was lost in a single, large step, consistent with intron release (Figure 4C, top). The apparent 57% − 11% = 46% splicing yield was comparable to what was observed in ensemble reactions on unlabeled *RPS30A* pre-mRNA (Figure 1D, bottom), suggesting both that the intron fluorophores did not significantly impair splicing and that fluorescence loss was an accurate reporter of splicing.

To examine U1 and U2 dynamics on pre-mRNAs that ultimately spliced, we picked 54 single-molecule records where most of the intron fluorescence abruptly disappeared in a single step, indicative of splicing. We ordered the records by the time of intron departure and plotted the binding of fluorescent U1 and U2 to each of these pre-mRNA molecules as a horizontal bar in a multicolor rastergram (Figure 4D). This rastergram revealed key features of spliceosome assembly and splicing. First, prior to intron departure, both U1 and U2 were observed to bind to

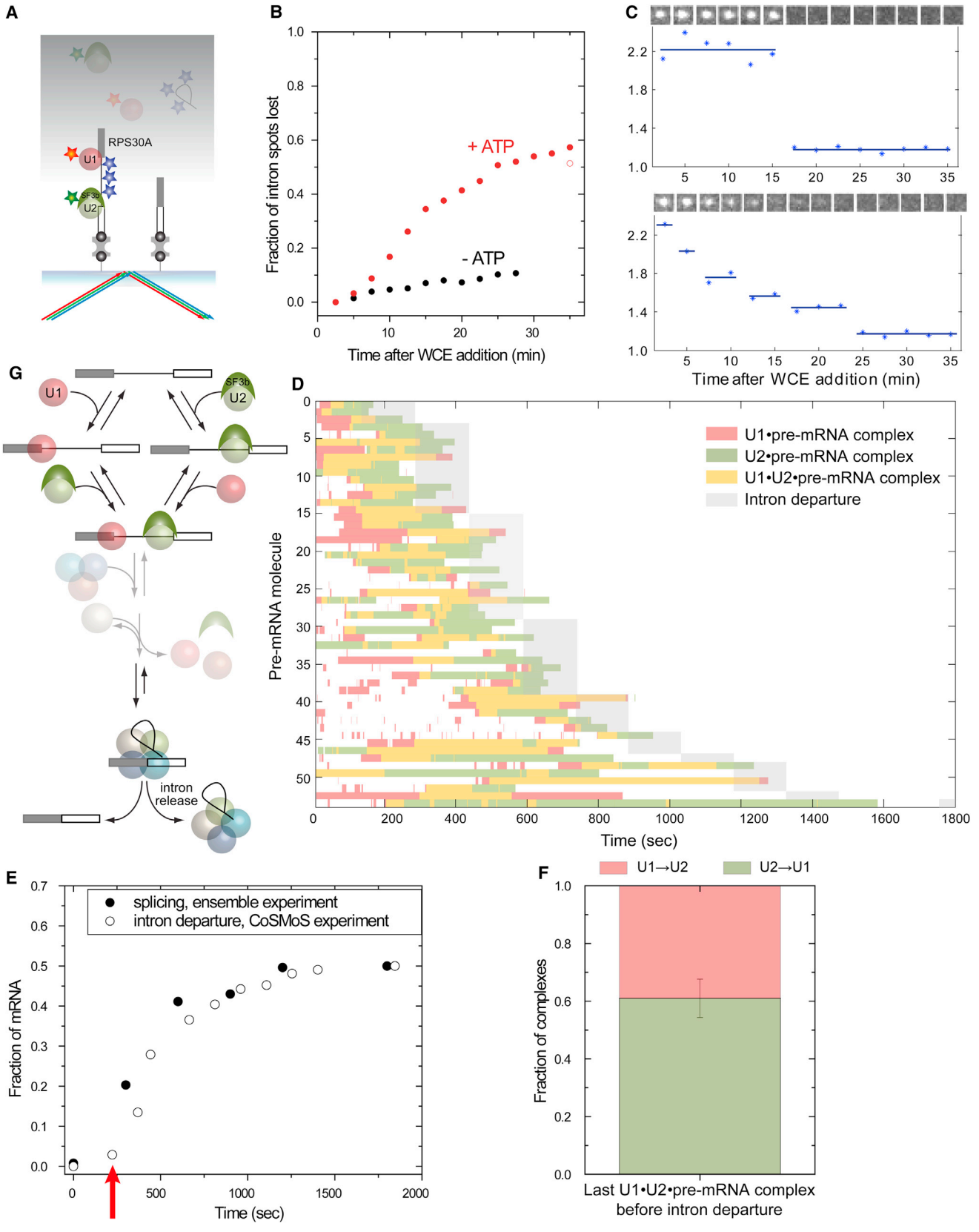


*(legend on next page)*

all pre-mRNA molecules. Subsequent to intron departure, however, essentially no U1 or U2 binding events were detected on any of the pre-mRNA molecules in this data set. Thus, neither U1 nor U2 detectably interact with the 114 nt spliced exon product complex, suggesting that their binding is exquisitely dependent on the presence of the intron. Second, the rate of intron release in this single-molecule assay was remarkably similar to the rate of second step chemistry determined in our ensemble assays (Figure 4E). Thus, intron release occurs quickly after second-step chemistry during *RPS30A* pre-mRNA splicing. Finally, in the single-molecule experiment, we observed an apparent lag in intron release of ~200 s (Figure 4E, arrow). This is consistent with the presence of multiple partially rate-limiting steps in the process of initial spliceosome assembly and activation (Hoskins et al., 2011).

Examination of the dynamics of U1 and U2 binding prior to intron release (Figure 4D) confirmed that many of the features we observed for the entire population of *RPS30A* molecules were shared by the subset of *RPS30A* pre-mRNA molecules destined to splice (46%; Figures 1D, bottom, and 2D). Even on the molecules destined to splice, U1 was highly dynamic, with an average of 4.4 binding events per pre-mRNA molecule (236 events observed on 54 molecules). In contrast, U2 was far less dynamic on the pre-mRNA molecules destined to splice: the average number of binding events per molecule (56 events observed on 54 molecules) was less than for U1. Most importantly, roughly half of all U1•U2•pre-mRNA prespliceosome formation events that preceded intron loss on *RPS30A* occurred by binding U2 before U1 (Figure 4F), similar to the fraction of *RPS30A* prespliceosome formation events that preceded U5 binding (Figure 3F). Taken together, these data clearly support the existence of a branched pathway in which functional spliceosomes can form by either a U1-first or a U2-first mechanism. They further suggest that the branches come together at the prespliceosome stage (Figure 4G), as both branches produce functionally (and likely structurally) identical prespliceosomes.

## DISCUSSION

Spliceosome assembly in *S. cerevisiae* has been understood to be a highly ordered process progressing linearly through a series of intermediate complexes culminating in a catalytically active spliceosome (Figure 1A). This model was based largely on the order of stable complexes observable in ensemble biochemical reactions. But not all stable complexes are necessarily on-pathway for active spliceosome assembly. Further, key transient intermediates and branched pathways can be difficult to detect in ensemble assays.

In the current work, we developed single-molecule methodologies to allow for the real-time observation of up to three different molecular species binding to and dissociating from a surface-tethered RNA molecule in a crude cell lysate. This three-way CoSMoS allowed us to identify on-pathway spliceosome assembly intermediates occurring in unperturbed splicing reactions on nonmutant pre-mRNAs. We examined the order of U1, U2, and U5•U4/U6 tri-snRNP binding to a broad set of yeast introns of varying length and sequence. These experiments reveal that the mechanism of U1 and U2 recruitment is not linear but occurs by a branched pathway that converges at the prespliceosome stage. Further, U1 binding was highly dynamic on all pre-mRNAs examined. This readily reversible U1 binding, coupled with the existence of multiple pathways for the initial assembly of functional spliceosomes, suggests that alternative splicing regulation in higher eukaryotes (particularly alternative 5′ splice site choice) likely involves modulation of the fractional flux along multiple assembly pathways that are in kinetic competition.

### A Branched Pathway for Prespliceosome Formation

The previous model that yeast prespliceosome assembly occurs entirely via a U1-first pathway was largely based on the following data from in vitro splicing reactions: (1) the most rapidly observable complexes formed on a well-spliced pre-mRNA contain U1 snRNA, but not other snRNAs (Ruby and Abelson, 1988); (2) stable U1 snRNP binding to the 5′ SS can occur in the absence of ATP, whereas stable binding of other snRNPs requires ATP (Ruby and Abelson, 1988); (3) stable association of U2 and U5 snRNPs with a pre-mRNA requires intact U1 snRNA (Ruby and Abelson, 1988); and (4) a portion of radioactive pre-mRNA molecules preincubated in splicing extracts incapable of forming U2-containing complexes (because they lacked either ATP or intact U2 snRNP) was found to be stably associated with U1 snRNP in "commitment complexes" that could be subsequently

**Figure 4. Splicing of *RPS30A* Pre-mRNAs through Alternative Prespliceosome Assembly Pathways**

(A) Experimental design. Binding of labeled U1 and U2 was visualized with red and green excitation. The intron of each pre-mRNA molecule was labeled with eight dye molecules on average; intron release was detected as loss of blue-excited fluorescence.

(B) Fraction of intron fluorescent spots lost from a single field of view at various times after adding WCE with ATP (red; n = 923) or without ATP (black; n = 1,272). The open red symbol is a photobleaching-independent estimate (average n = 474 ± 12 spot per field of view after 35 min; see Experimental Procedures).

(C) Time records of intron fluorescence loss in WCE + ATP. Top: an example of fluorescence loss that occurs in a single step, presumably due to splicing. Bottom: fluorescence loss in multiple steps, presumably due to photobleaching. Insets: a gallery of the images (1.34 × 1.34 μm) corresponding to each time point is shown.

(D) Rastergram summarizing the presence of fluorescent U1 (red), U2 (green) snRNPs, or both (yellow) on individual *RPS30A* pre-mRNA molecules. Only pre-mRNAs that were observed to lose intron fluorescence in a large step, presumably due to the intron departure, were selected for analysis (n = 54). Records are ordered by the time interval in which intron departure occurred (shading).

(E) Time courses of intron departure (open symbols; from CoSMoS experiment) and the second step of splicing (filled symbols; from ensemble experiment). The red arrow indicates an apparent lag in the intron departure detected in the CoSMoS experiments (see text).

(F) Genesis of the U1•U2•pre-mRNA complex that most closely preceded intron departure from each pre-mRNA molecule in (D). Fractions (±SE) of complexes formed through the U1→U2 (red) or U2→U1 (green) pathways are indicated.

(G) Summary of the pathways observed in this experiment. Catalysis of splicing and subsequent intron release can occur through prespliceosomes assembled by both U1→U2 and U2→U1 branches.

chased into active spliceosomes, even when challenged with a large excess of unlabelled competitor pre-mRNA (Legrain et al., 1988; Seraphin and Rosbash, 1989).

Whereas the above studies were instrumental in pioneering our understanding of the major steps in initial spliceosome assembly, such ensemble studies are largely restricted to the detection and analysis of stable species in stalled splicing reactions. Therefore, such results are consistent with multiple possible assembly pathways. By allowing us to study the dynamics of both short- and long-lived interactions with individual pre-mRNA molecules in unperturbed splicing reactions, our CoSMoS technology allows us to directly follow the pathway of individual assembly events. Using two-color WCEs, we previously reported (Hoskins et al., 2011) that *RP51A* pre-mRNA exhibits highly ordered (~90% or more) U1→U2 binding. The experiments with three-color WCEs reported here further refined this analysis by allowing us to focus on the subset of U1 and U2 binding events that are productive in the sense that they are directly followed by U5•U4/U6 tri-snRNP addition. Because the first U1 binding to *RP51A* is 3.3-fold faster than U5 binding (Figure 2E) and is much more dynamic (with on average 3.5 U1 versus 0.9 U5 long-lived events [≥1.5 s] per *RP51A* pre-mRNA molecule during the first 20 min of the experiment; Figure 2D), many U1 binding events are necessarily unproductive for subsequent U5 recruitment. Nonetheless, when only U1 binding events productive for subsequent U5 binding were considered, a large fraction (>80%) still proceeded through the U1→U2→U5 pathway on *RP51A* pre-mRNA (Figure 3F). Thus, our current data are consistent with our previous report that *RP51A* exhibits largely ordered U1→U2 binding. However, the improved methods developed for the present study (see Experimental Procedures) show clearly that a fraction (<20%) of *RP51A* pre-spliceosomes do in fact assemble by the U2-first pathway.

Coincidentally, of all six pre-mRNAs for which we performed three-way CoSMoS experiments, the *RP51A* pre-mRNA examined in our earlier study exhibited the greatest fractional flux through the U1→U2→U5 pathway and the least through the U2→U1→U5 pathway. In contrast, the U2→U1→U5 pathway was more prevalent on each of the other five pre-mRNAs in our set, with *UBC4* and *RPS30A* exhibiting the most fractional flux through the U2→U1→U5 pathway (Figure 3F). Thus, different pre-mRNA species utilize the alternative branches to different extents, possibly because of differences in the relative rates of U1 and U2 binding to or dissociation from the pre-mRNA species. The pre-mRNA-specific kinetics may reflect differential 5′ SS and BS accessibilities due to internal RNA structures and/or differential association kinetics of these sites with factors (e.g., branchpoint-binding protein) present in the WCE. These kinetic differences in snRNP recruitment in vitro may explain in part the previously reported in vivo transcript-specific effects of mutations in the core splicing machinery (Pleiss et al., 2007).

## Unifying the In Vitro and In Vivo Spliceosome Assembly Models

During transcription in vivo, the 5′ SS of a pre-mRNA molecule is necessarily synthesized before the BS and 3′ SS. Consistent with this, ChIP experiments in budding yeast have shown that U1 signal accumulates along the entire length of introns in vivo, whereas U2 and U5 signals are skewed toward intron 3′ ends (Görnemann et al., 2005; Moore et al., 2006; Tardiff et al., 2006). These data could be interpreted as supporting a highly ordered, U1-first spliceosome assembly mechanism. However, fluorescence recovery after photobleaching experiments in mammalian cells indicate that U1 is ~10-fold more mobile in vivo than the other spliceosomal subcomplexes (Huranová et al., 2010). Further, the cold-sensitive phenotype observed in yeast upon lengthening (hyperstabilization) of the U1/5′ SS duplex suggests that efficient splicing in vivo requires that the U1/5′ SS interaction be relatively weak (Staley and Guthrie, 1999). All of these results are consistent with our CoSMoS data, indicating highly dynamic U1 binding in vitro (Figures 2D and 4D; Hoskins et al., 2011). Thus, 5′ SSs on nascent transcripts may be subject to numerous U1 arrivals and departures prior to synthesis and appearance of the downstream BS and 3′ SS. This means that the particular U1 molecule that participates in productive cross-intron interactions with U2 on a nascent transcript in vivo may well have bound the 5′ SS after U2 arrived at the BS (Figure 5A).

In vertebrates, where most genes contain multiple introns that are much longer than internal exons, initial spliceosome assembly is thought to initiate by "exon definition," wherein cross-exon interactions facilitate initial U2 and U1 recruitment to exon ends (Robberson et al., 1990). Subsequent cross-intron interactions then pair these species with independently recruited U1 and U2 bound to adjacent exons. Thus, in higher eukaryotes, independent recruitment of the U1 and U2 snRNPs at opposite intron ends is likely the predominant spliceosome assembly pathway. The data presented here showing that functional spliceosome assembly in yeast can also occur by independent recruitment of U1 and U2 at intron ends thus resolve long-standing inconsistencies between the exon definition model of spliceosome assembly supported by the in vivo effects of splice site and exon mutations in higher eukaryotes (Moldón and Query, 2010; Roca et al., 2013) and the "spliceosome cycle" model, based largely on the series of stable complexes observable in in vitro splicing reactions (Moore et al., 1993; Ruby and Abelson, 1991; Wahl et al., 2009).

## Rethinking the Spliceosome Cycle

Given the existence of a branched pathway for U1 and U2 addition, are there other noncanonical pathways for subsequent steps in spliceosome assembly? In our experiments in yeast WCE, almost all U5 binding events occurred subsequent to formation of a U1•U2•pre-mRNA complex. Thus, U5•U4/U6 tri-snRNP recruitment to yeast introns apparently requires prior recruitment of both U1 and U2. This result is consistent with previous data showing that blocking or cleaving the portions of U1 and U2 snRNAs that base pair with the 5′ SS and BS, respectively, completely abrogates stable tri-snRNP recruitment (Ruby and Abelson, 1988). Although spliceosome assembly in human extracts is similarly blocked by degrading U2 snRNA (Krainer and Maniatis, 1985), human extracts supplemented with serine/arginine-rich (SR) proteins are capable of splicing, even in the absence of U1 snRNP (Crispino et al., 1994; Konforti et al., 1993; Tarn and Steitz, 1994). This difference between the

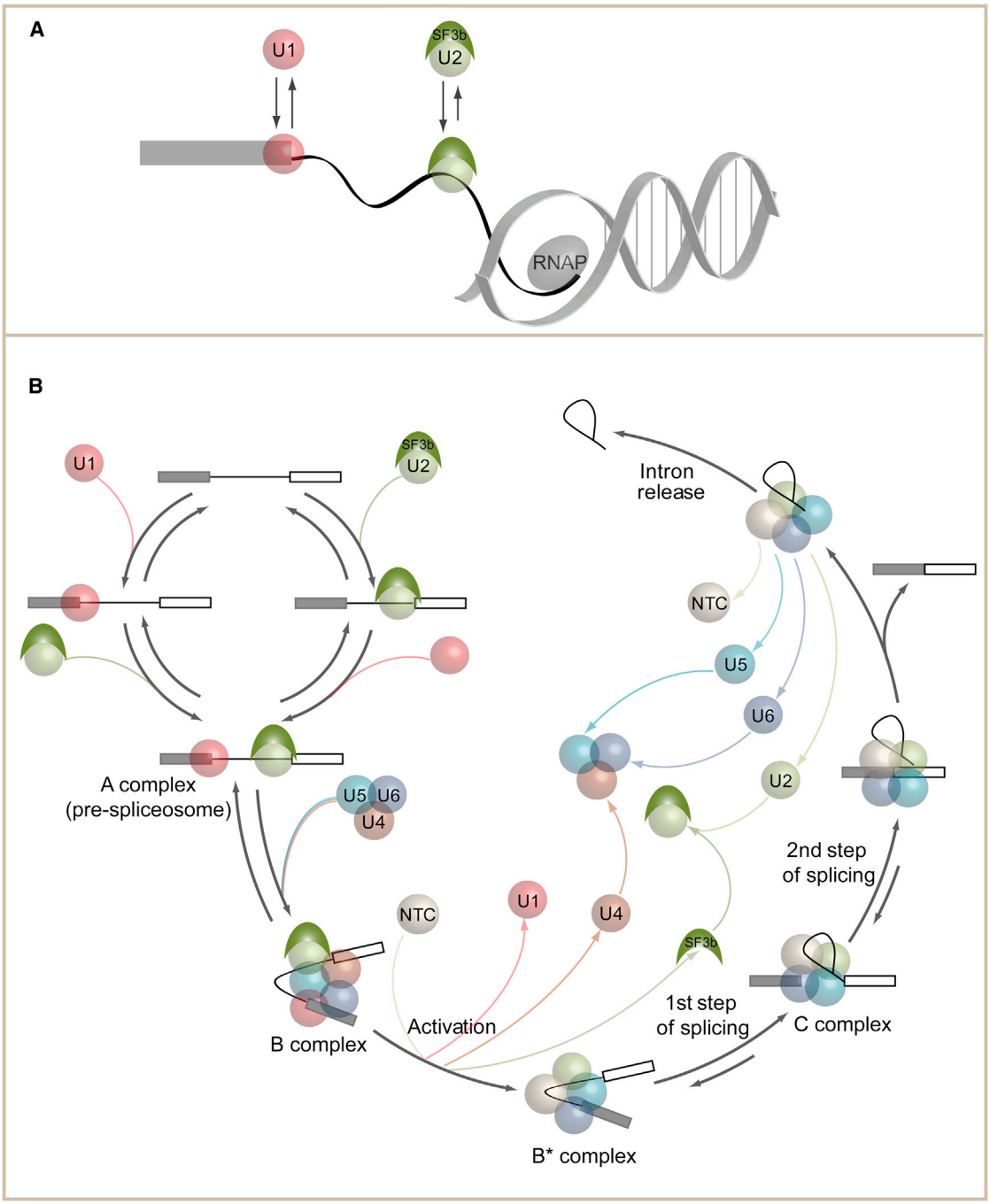


**Figure 5. Implications of Alternative Pathways for U1 and U2 Addition**

(A) Cotranscriptional prespliceosome formation. RNA polymerase II (RNAP) transcribes the 5′ SS before the BS, providing U1 an opportunity to bind prior to U2, but this may not dictate which binds first to form the prespliceosome (see text).

(B) Spliceosome cycle—2013. Overall pathway for yeast spliceosome assembly, activation, and splicing incorporating both U1 → U2 and U2 → U1 branches and known reversibilities is shown (Hoskins et al., 2011; Tseng and Cheng, 2008).

yeast and mammalian systems likely reflects additional positive interactions in the mammalian system between the core splicing machinery and non-snRNP splicing factors bound to exonic and intronic splicing enhancer elements (reviewed in Fukumura and Inoue [2009] and Roca et al. [2013]).

More recent data suggest even greater flexibility for mammalian spliceosome assembly. For example, the polypyrimidine tract recognition factor U2AF, which functions to recruit U2 snRNP to mammalian BS sequences, was recently shown to physically associate with both the NTC and the phosphorylated

C-terminal domain of RNA polymerase II (David et al., 2011). Thus, on some mammalian introns, U2AF and the NTC are likely recruited cotranscriptionally and prior to U5•U4/U6 tri-snRNP recruitment. Another study reported purification of an in vitro assembled cross-exon complex thought to represent an exon definition complex; mass spectroscopy analysis revealed it to contain U1, U2, and U5•U4/U6 tri-snRNP components (Schneider et al., 2010). This purified cross-exon complex could be converted into a cross-intron B-like spliceosomal complex by the addition of a 5′ SS-containing oligonucleotide. The oligonucleotide presumably bound the U5 and U6 snRNAs in the cross-exon complex directly without ever engaging in a base pairing interaction with U1 snRNA (which in the cross-exon complex was paired with the 5′ SS at the other end of the exon). Thus, in higher organisms, the predominant mode of spliceosome assembly on long introns separating short exons may be initial NTC and U5•U4/U6 tri-snRNP recruitment to cross-exon complexes, which are then converted to cross-intron spliceosomes, bypassing any requirement for a cross-intron U1•U2 prespliceosome.

Thus, both the above studies and our single-molecule data show that spliceosome assembly is more flexible and dynamic than is suggested by the canonical spliceosome cycle (Moore et al., 1993; Ruby and Abelson, 1991; Wahl et al., 2009). Our single-molecule data examining the order of U1, U2, and U5•U4/U6 tri-snRNP arrival suggest that the yeast spliceosome cycle should simply be updated by adding a branched pathway for U1 and U2 addition (Figure 5B). However, the full scope of mammalian spliceosome assembly pathways is likely not amenable to depiction in any single schematic. Importantly, the existence of multiple alternative and reversible assembly pathways has profound consequences for our understanding of alternative splicing regulation. Our data suggest that alternative splice site choice may involve kinetic modulation of alternative assembly pathways. Therefore, full understanding of how splice site selection is governed during alternative splicing will now require elucidation of the kinetically competent spliceosome assembly pathway(s) functioning on individual splice site pairs under specific cellular conditions. Whereas in vitro studies such as ours may reveal a more complete spectrum of possible assembly pathways, elucidating which pathways are relevant in vivo and how the fractional flux through each pathway is modulated to regulate alternative splicing will necessitate development of methods capable of assessing spliceosome assembly dynamics at the single-molecule level in living cells.

## EXPERIMENTAL PROCEDURES

### Preparation of the Pre-mRNAs

Capped pre-mRNAs were produced in vitro by T7 RNA polymerase transcription (Crawford et al., 2008). The template for T7 RNA polymerase was prepared by PCR from yeast genomic DNA of strain BJ2168 using a forward primer encoding the T7 promoter followed by GG and a segment of the gene of interest. The gene segment consisted of the entire first exon, the entire intron, and 50 nucleotides of the second exon (see Supplemental Experimental Procedures).

The pre-mRNAs for ensemble splicing assays were $^{32}$P-labeled as described (Crawford et al., 2008). The pre-mRNAs for the single-molecule experiments were prepared using T4 RNA ligase 1 (New England Biolabs) by splinted ligation of the 5′ capped pre-mRNA to a biotinated 2′-O-methyl oligonucleotide (5′-mAmUmCmCmGmGmAmGmCmGmAmGaaU*mAmGmA-biotin-3′, where aaU* (5(3-aminoallyl)-uridine) was labeled with either Alexa647 or Alexa488 (Crawford et al., 2008).

The intron-labeled *RPS30A* pre-mRNA was constructed from three transcripts (see Supplemental Experimental Procedures) by splinted ligation with T4 RNA ligase 1 (Moore and Query, 2000) to produce the intron-labeled *RPS30A* pre-mRNA. Several 5-(3-aminoallyl)-uridine triphosphates (UTPs) were incorporated in the transcript comprising the middle part of the intron and were posttranscriptionally labeled with Alexa488 tetrafluorophenyl ester (ARES DNA labeling kit, Invitrogen, Molecular Probes). The 3′ transcript was biotinylated posttranscriptionally using splint-directed extension by Klenow fragment (3′→5′ exo$^-$; New England Biolabs). All pre-mRNAs were purified from a denaturing electrophoresis gel. On average, eight Alexa488 dye moieties per intron-labeled *RPS30A* were spectrophotometrically detected (see Supplemental Experimental Procedures).

### Preparation of Yeast Strains

Preparation of the yeast strains used to monitor binding of single-spliceosomal subcomplexes (Figures 2 and S1A) was described previously (Hoskins et al., 2011). In each of these strains, two of the subcomplex proteins were tagged with C-terminal eDHFR (*E. coli* dihydrofolate reductase) tags: SNP1 and PRP40 in U1 snRNP; CUS1 and HSH155 in U2 snRNP; SNU114 and BRR2 in U5 snRNP; and CEF1 and NTC90 in NTC.

The yeast strain to simultaneously monitor U1, U2, and U5 binding (Figures 3 and S2) bears C-terminal eDHFR tags on SNP1 and PRP40 of U1 snRNP (Hoskins et al., 2011), a C-terminal SNAP$_f$ tag of BRR2 (U5 snRNP), and a C-terminal CLIP$_f$ tag on CUS1 (U2 snRNP). All tags were linked to their respective proteins through (Gly-Ser-Gly)$_2$ linkers (see the Supplemental Experimental Procedures).

Preparation of the yeast strain with U1 and U2 snRNPs labeled with fluorophores of different colors (Figures 4 and S1B) was described previously (Hoskins et al., 2011). U1 proteins SNP1 and PRP40 were tagged with eDHFR tags, and the U2 protein CUS1 was tagged with the SNAP tag on their C termini.

### Preparation of Yeast Whole-Cell Splicing Extracts

Yeast WCEs were prepared as previously described (Crawford et al., 2008) from yeast cultures grown to optical density at 590 nm ($OD_{590}$) 1.5–1.8. For strains that contained only eDHFR tags, the WCE was aliquoted and frozen in liquid nitrogen after the dialysis.

For the yeast strains containing SNAP, SNAP$_f$, and/or CLIP$_f$ tags in addition to the eDHFR tags, the fluorophore(s) (SNAP-Surface 549 for the SNAP tag, SNAP-Surface 488 for the SNAP$_f$ tag, and CLIP-Surface 547 for the CLIP$_f$ tag) were added to the WCE to a final concentration of 1 to 2 μM after the high-speed centrifugation step. The labeling reaction was carried out at room temperature (24°C) for 30 min in the dark. Excess dye was removed by gel filtration through Sephadex G-25 (Hoskins et al., 2011). Aliquots of the dye-labeled WCE were frozen in liquid nitrogen.

The activity of each WCE was tested (after labeling the SNAP, SNAP$_f$, and CLIP$_f$ tags when present) in an ensemble splicing assay. Only WCE fractions with splicing activities comparable to that of the wild-type WCE were used in the single-molecule experiments.

WCE was thawed immediately before use. All extracts that contained eDHFR tags were used with added Cy3- or Cy5-trimethoprim (TMP) conjugates that were synthesized in the laboratory of Virginia Cornish, as described in Hoskins et al. (2011). The TMP conjugates were added to the splicing mix to a final concentration of 20 nM immediately before loading it into the flow chamber for single-molecule microscopy.

### Ensemble Experiments

The rates and yields of the first and second step reactions were detected in ensemble experiments in which pre-mRNA (trace labeled with α-$^{32}$P-UTP) was incubated with WCE in the presence of ATP for 0–60 min. Products of the first and second step were visualized by denaturing PAGE. The radioactivity in pre-mRNA, lariat intron intermediate, and spliced exon bands was quantified by phosphorimaging and divided by the number of uridines present in the corresponding species to yield the relative concentrations *Rp, Rl*, and

*Re,* respectively. The fraction of the RNA molecules that accomplished first (*f*1) and second (*f*2) step of splicing was calculated as

$$f1 = \frac{Rl + Re}{Rl + Re + Rp}$$

$$f2 = \frac{Re}{Rl + Re + Rp}.$$

The time dependence of *f*1 and *f*2 was plotted and fit to a single exponential function with a time offset *t*0 and asymptote *f*0,

$$f(t) = f0\left(1 - e^{-k(t-t0)}\right),$$

to determine the apparent rates *k* of the first and second chemical steps, respectively.

## Single-Molecule Experiments

The slides and the coverslips for flow chambers were plasma cleaned under argon plasma (Selvin et al., 2007). The chambers were constructed and treated with polyethylene glycol (PEG)/biotin-PEG and streptavidin (Crawford et al., 2008). Biotinated pre-mRNAs were tethered to the chamber surface at low densities (typically 0.2–0.5 fluorescent spots $\mu m^{-2}$). Custom-made micromirror total internal reflection fluorescence (TIRF) microscopes (Friedman et al., 2006) with modifications (Hoskins et al., 2011) were used to acquire images. The microscope fields of view ranged between 314 $\mu m^2$ and 3,250 $\mu m^2$.

The splicing reaction was initiated at room temperature (24°C) by introducing into the flow chambers 40% WCE containing fluorophore-labeled proteins in splicing buffer (Crawford et al., 2008). Introduction of the solution was done either manually (dead time 30–120 s) or with the use of the syringe pump (dead time <~20 s; Hoskins et al., 2011). The latter method was used to initiate the splicing reaction in all experiments in which binding of fluorophore-labeled U1 snRNP was monitored. A photoprotection system based on *Pseudomonas* protocatechuate dioxygenase (Crawford et al., 2008) and 1 mM Trolox (Dave et al., 2009; Hoskins et al., 2011; Rasnik et al., 2006) were used in all the experiments. In the experiments where SNAP-Surface 488 (blue) dye was imaged, additional triplet quenchers cyclooctatetraene and 4-nitrobenzyl alcohol were included to final concentrations of 1 mM (Dave et al., 2009; Hoskins et al., 2011; Rasnik et al., 2006). For most experiments, ATP was added to a final concentration of 2 mM. For experiments conducted in the absence of ATP, the WCE was depleted of ATP (Hoskins et al., 2011).

During the experiments that monitored binding of individual spliceosomal subcomplexes to surface-tethered pre-mRNAs, Cy3-TMP-labeled (green fluorophore) subcomplex fluorescence was imaged once every 1.4–1.5 s by excitation at 532 nm (green laser; 1 s frame duration). Once every 50–75 s, the subcomplex imaging was interrupted, the microscope was automatically refocused (Hoskins et al., 2011), and the Alexa647-labeled (red fluorophore) pre-mRNA molecules were imaged by excitation at 633 nm (red laser; one frame of 1 s duration). Control experiments (Hoskins et al., 2011) demonstrated that few spots of subcomplex fluorescence were observed in the absence of surface-tethered RNA.

In experiments with the intron-labeled *RPS30A* pre-mRNA, we used an extract doubly labeled with Cy5-TMP (red fluorophore) on U1 snRNP and SNAP-Surface 549 (green fluorophore) on U2 snRNP. Samples were imaged (1 s frame durations) by continuous excitation at 532 nm (green laser) and 633 nm (red laser). Once every 2.5 min, the U1 and U2 excitation and imaging was interrupted, the microscope was automatically refocused, and a single frame of intron fluorescence by excitation at 488 nm (blue laser) was acquired. To formulate a photobleaching-independent estimate of the fraction of unspliced introns remaining at the end of the 35-min-long incubation in WCE plus 2 mM ATP experiment (Figure 4B, open red symbol), we measured the intron fluorescent spot surface density in eight additional fields of view that were not exposed to any laser excitation earlier in the experiment.

For the experiments in which U1, U2, and U5 were labeled with fluorophores of different colors, the surface density of Alexa488-labeled pre-mRNA molecules was first checked using the fluorescence from the Alexa488 label (blue fluorophore). The Alexa488 label was then photobleached completely by exposure to 488 nm (blue laser) excitation in the absence of photoprotection reagents. We then introduced extract that was labeled with Cy5-TMP (red fluorophore) on U1 snRNP, CLIP-Surface 547 (green fluorophore) on U2 snRNP, and SNAP-Surface 488 (blue fluorophore) on U5 snRNP. U1 and U2 were imaged simultaneously by excitation at 532 nm (green laser) and 633 nm (red laser) either continuously (Figure 3F) or three continuous frames every 6 s (Figures 3C and 3D; 1 s frame durations in each case). The U1 and U2 excitation and imaging was interrupted once every 6 (Figures 3C and 3D) or 10 s (Figure 3F) to automatically focus and acquire a single 1 s duration image of U5 using excitation at 488 nm (blue laser). Each field of view included several surface-bound fluorescent beads (TransFluoSpheres streptavidin-labeled, 0.04 μm [488/645], Invitrogen). Bead locations were measured and used to correct for stage drift. The locations of the pre-mRNA molecules on the surface in these records were taken to be all locations at which binding of U1 was observed, because surface binding of U1 in a control sample in which no pre-mRNA was present was ≤1% that in experimental samples (0.0009 versus 0.08–0.12 fluorescent U1 spots $\mu m^{-2}$ averaged over all the fames in a recording).

## Data Analysis

Analysis of CoSMoS data were performed using custom programs implemented in MATLAB (The Mathworks). Intensity of labeled snRNP fluorescence at the position of each pre-mRNA molecule was integrated over a 3 × 3 or 5 × 5 pixel region and baseline corrected as described (Hoskins et al., 2011). Spliceosomal subcomplex binding events were scored using previously reported methods (Hoskins et al., 2011). The presence of two dye moieties on U1 snRNP enabled an emission intensity analysis (Hoskins et al., 2011) that confirmed that 71% ± 3% of fluorescent U1 snRNPs contained two dyes. The fraction of nonfluorescent U1 snRNPs in triply labeled WCE could thus be estimated as 8.4%. For U1 snRNPs labeled with two dyes, 81.5% ± 3% of recorded U1 binding events involved simultaneous arrival of the two fluorescent U1 proteins, indicating that most of the observed binding events report on the recruitment of U1 snRNP rather than free proteins. Further, glycerol gradient sedimentation of the triply labeled WCE demonstrated that practically all of fluorescently labeled CUS1 is part of U2 snRNP (Figure S2E). The analysis of the emission intensities from U2 snRNP (which was labeled with a single-dye moiety) indicated that nearly all of the pre-mRNA molecules that assembled the spliceosome via U2 → U1 → U5 pathway were not observed to bind a second U2 snRNP when one was already bound (96% for *RPS30A* pre-mRNA, n = 122). The times to the first binding event (Figure 2E) were averaged for all pre-mRNAs that were observed to bind a spliceosomal subcomplex in each experiment where a single spliceosomal complex was fluorescently labeled.

In our previous study (Hoskins et al., 2011), we used WCE, in which U1 and U2 were labeled to determine the order of U1 and U2 binding by finding the first U2 binding event in a record and then finding the U1 binding event that was closest in time and recording whether this U1 event was before or after the U2 event. In the present study, we refined these analysis methods in two important ways. First, in the present study, we confined our analysis to molecules that were observed to bind U5 (Figure 3) or for which intron departure was observed (Figure 4). This reduced or eliminated spurious data from the subpopulation of pre-mRNAs in the data set that were trapped in dead-end complexes (Hoskins et al., 2011). Second, in the present study, we scored formation of a U1•U2•pre-mRNA complex only when we observed both U1 and U2 fluorescence present simultaneously on the same pre-mRNA molecule, rather than merely requiring their sequential presence, as in the earlier study. This may have removed a small number of events in which the U1 and U2 molecules were not simultaneously present on the pre-mRNA and therefore did not form a prespliceosome. In particular, in the experiment shown in Figure 3, we tabulated each U5 binding event that was preceded in the data record by a time interval in which a U1•U2•pre-mRNA complex was present, as judged by observation of simultaneously present U1 and U2 fluorescence. For U5 events that were preceded by multiple intervals in which U1 and U2 were both present, only the interval that most closely preceded U5 binding was included. If two or more U5 binding events were detected after the formation of a given U1•U2•pre-mRNA complex, only the earliest of these was included. For the tabulated pairs of U1•U2 and U5 events, the time of the first frame in which U5 was detected was defined as $t_{U5}$ and the time of the first frame in which

both U1 and U2 fluorescent spots were simultaneously present was defined as $t_{U1 \cdot U2}$ (e.g., see Figure 3C). Each pair was classified based on the order of U1 and U2 arrival (e.g., see Figure 3F): as "U1→U2" for events in which U2 appearance coincided with $t_{U1 \cdot U2}$; as "U2→U1" for events in which U1 appearance coincided with $t_{U1 \cdot U2}$; and as "$t_{U1}$=$t_{U2}$" for events in which U1 and U2 appearances were simultaneous within the experimental time resolution. For events in each classification, the delay times $t_{U5} - t_{U1 \cdot U2}$ were calculated and the probability density distribution plot (Figure 3D) was constructed by binning the delay times and dividing the number of observations in each bin by both the total number of events in the group and by the width of the bin. The unbinned data were fit (Figure 3D, lines) with a one-parameter single exponential function using a maximum likelihood algorithm (Hoskins et al., 2011) to yield the apparent first order rate constant for U5 snRNP binding to the prespliceosomal complex. The standard error of the rate constant was estimated by bootstrapping (Hoskins et al., 2011).

For the experiments with labeled intron (Figure 4), we selected only pre-mRNA molecules that displayed intron departure as judged by (1) loss of intron fluorescence in a single step in intensity that was judged to be larger than that observed for photobleaching of a single-dye moiety or (2) loss of intron fluorescence in multiple steps, the last of which was judged to be at least twice the size of single-dye photobleaching steps observed earlier in the same pre-mRNA molecule. Once these intron loss events were identified, the preceding prespliceosome formation event was identified and classified with respect to the order of U1 and U2 binding in a manner analogous to that described for the Figure 3 experiment. The time course of intron departure (Figure 4E) was normalized based on the assumption that the fraction of pre-mRNA molecules that displayed intron departure by 1,844 s (CoSMoS experiment) was equal to the fraction that performed the second chemical step of splicing by 1,800 s (ensemble experiment).

## SUPPLEMENTAL INFORMATION

Supplemental Information includes Extended Experimental Procedures and two figures and can be found with this article online at http://dx.doi.org/10.1016/j.celrep.2013.08.026.

## ACKNOWLEDGMENTS

We thank R. Wombacher, S. Gallagher, and V. Cornish for Cy3-TMP and Cy5-TMP analogs. We thank E. Anderson, J. Chung, N. Ramirez, B. Smith, A. Okonechnikov, J. Yan, and E. Heyer for helpful discussions and technical assistance. This work was supported by NIH R01 GM043369 (to J.G.), GM81648 (to J.G.), GM53007 (to M.J.M.), and K99/R00 GM86471 (to A.A.H.). M.J.M. is a Howard Hughes Medical Institute Investigator. I.R.C.J. and M.-Q.X. are employees of New England Biolabs.

Received: February 19, 2013
Revised: July 18, 2013
Accepted: August 15, 2013
Published: September 26, 2013

## REFERENCES

Abelson, J., Blanco, M., Ditzler, M.A., Fuller, F., Aravamudhan, P., Wood, M., Villa, T., Ryan, D.E., Pleiss, J.A., Maeder, C., et al. (2010). Conformational dynamics of single pre-mRNA molecules during in vitro splicing. Nat. Struct. Mol. Biol. *17*, 504–512.

Crawford, D.J., Hoskins, A.A., Friedman, L.J., Gelles, J., and Moore, M.J. (2008). Visualizing the splicing of single pre-mRNA molecules in whole cell extract. RNA *14*, 170–179.

Crispino, J.D., Blencowe, B.J., and Sharp, P.A. (1994). Complementation by SR proteins of pre-mRNA splicing reactions depleted of U1 snRNP. Science *265*, 1866–1869.

Dave, R., Terry, D.S., Munro, J.B., and Blanchard, S.C. (2009). Mitigating unwanted photophysical processes for improved single-molecule fluorescence imaging. Biophys. J. *96*, 2371–2381.

David, C.J., Boyne, A.R., Millhouse, S.R., and Manley, J.L. (2011). The RNA polymerase II C-terminal domain promotes splicing activation through recruitment of a U2AF65-Prp19 complex. Genes Dev. *25*, 972–983.

Fink, G.R. (1987). Pseudogenes in yeast? Cell *49*, 5–6.

Friedman, L.J., Chung, J., and Gelles, J. (2006). Viewing dynamic assembly of molecular complexes by multi-wavelength single-molecule fluorescence. Biophys. J. *91*, 1023–1031.

Fukumura, K., and Inoue, K. (2009). Role and mechanism of U1-independent pre-mRNA splicing in the regulation of alternative splicing. RNA Biol. *6*, 395–398.

Görnemann, J., Kotovic, K.M., Hujer, K., and Neugebauer, K.M. (2005). Cotranscriptional spliceosome assembly occurs in a stepwise fashion and requires the cap binding complex. Mol. Cell *19*, 53–63.

Hoskins, A.A., and Moore, M.J. (2012). The spliceosome: a flexible, reversible macromolecular machine. Trends Biochem. Sci. *37*, 179–188.

Hoskins, A.A., Friedman, L.J., Gallagher, S.S., Crawford, D.J., Anderson, E.G., Wombacher, R., Ramirez, N., Cornish, V.W., Gelles, J., and Moore, M.J. (2011). Ordered and dynamic assembly of single spliceosomes. Science *331*, 1289–1295.

Huranová, M., Ivani, I., Benda, A., Poser, I., Brody, Y., Hof, M., Shav-Tal, Y., Neugebauer, K.M., and Stanek, D. (2010). The differential interaction of snRNPs with pre-mRNA reveals splicing kinetics in living cells. J. Cell Biol. *191*, 75–86.

Konforti, B.B., Koziolkiewicz, M.J., and Konarska, M.M. (1993). Disruption of base pairing between the 5′ splice site and the 5′ end of U1 snRNA is required for spliceosome assembly. Cell *75*, 863–873.

Kotlajich, M.V., Crabb, T.L., and Hertel, K.J. (2009). Spliceosome assembly pathways for different types of alternative splicing converge during commitment to splice site pairing in the A complex. Mol. Cell. Biol. *29*, 1072–1082.

Krainer, A.R., and Maniatis, T. (1985). Multiple factors including the small nuclear ribonucleoproteins U1 and U2 are necessary for pre-mRNA splicing in vitro. Cell *42*, 725–736.

Legrain, P., Seraphin, B., and Rosbash, M. (1988). Early commitment of yeast pre-mRNA to the spliceosome pathway. Mol. Cell. Biol. *8*, 3755–3760.

Matlin, A.J., and Moore, M.J. (2007). Spliceosome assembly and composition. Adv. Exp. Med. Biol. *623*, 14–35.

Moldón, A., and Query, C. (2010). Crossing the exon. Mol. Cell *38*, 159–161.

Moore, M.J., and Query, C.C. (2000). Joining of RNAs by splinted ligation. Methods Enzymol. *317*, 109–123.

Moore, M.J., Query, C.C., and Sharp, P.A. (1993). Splicing of Precursors to mRNA by the Spliceosome. In The RNA World, R.F. Gesteland, T.R. Cech, and J.F. Atkins, eds. (Cold Spring Harbor: Cold Spring Harbor Laboratory Press), pp. 303–357.

Moore, M.J., Schwartzfarb, E.M., Silver, P.A., and Yu, M.C. (2006). Differential recruitment of the splicing machinery during transcription predicts genome-wide patterns of mRNA splicing. Mol. Cell *24*, 903–915.

Pikielny, C.W., Rymond, B.C., and Rosbash, M. (1986). Electrophoresis of ribonucleoproteins reveals an ordered assembly pathway of yeast splicing complexes. Nature *324*, 341–345.

Pleiss, J.A., Whitworth, G.B., Bergkessel, M., and Guthrie, C. (2007). Transcript specificity in yeast pre-mRNA splicing revealed by mutations in core spliceosomal components. PLoS Biol. *5*, e90.

Rasnik, I., McKinney, S.A., and Ha, T. (2006). Nonblinking and long-lasting single-molecule fluorescence imaging. Nat. Methods *3*, 891–893.

Robberson, B.L., Cote, G.J., and Berget, S.M. (1990). Exon definition may facilitate splice site selection in RNAs with multiple exons. Mol. Cell. Biol. *10*, 84–94.

Roca, X., Krainer, A.R., and Eperon, I.C. (2013). Pick one, but be quick: 5′ splice sites and the problems of too many choices. Genes Dev. *27*, 129–144.

Ruby, S.W., and Abelson, J. (1988). An early hierarchic role of U1 small nuclear ribonucleoprotein in spliceosome assembly. Science *242*, 1028–1035.

Ruby, S.W., and Abelson, J. (1991). Pre-mRNA splicing in yeast. Trends Genet. *7*, 79–85.

Schneider, M., Will, C.L., Anokhina, M., Tazi, J., Urlaub, H., and Lührmann, R. (2010). Exon definition complexes contain the tri-snRNP and can be directly converted into B-like precatalytic splicing complexes. Mol. Cell *38*, 223–235.

Selvin, P.R., Lougheed, T., Tonks Hoffman, M., Park, H., Balci, H., Blehm, B.H., and Toprak, E. (2007). Constructing sample chambers for fluorescence imaging with one-nanometer accuracy (FIONA). Cold Spring Harb Protoc. Published online October 1, 2007. http://dx.doi.org/10.1101/pdb.prot4867.

Seraphin, B., and Rosbash, M. (1989). Identification of functional U1 snRNA-pre-mRNA complexes committed to spliceosome assembly and splicing. Cell *59*, 349–358.

Staley, J.P., and Guthrie, C. (1999). An RNA switch at the 5′ splice site requires ATP and the DEAD box protein Prp28p. Mol. Cell *3*, 55–64.

Staley, J.P., and Woolford, J.L., Jr. (2009). Assembly of ribosomes and spliceosomes: complex ribonucleoprotein machines. Curr. Opin. Cell Biol. *21*, 109–118.

Tarn, W.Y., and Steitz, J.A. (1994). SR proteins can compensate for the loss of U1 snRNP functions in vitro. Genes Dev. *8*, 2704–2717.

Tardiff, D.F., Lacadie, S.A., and Rosbash, M. (2006). A genome-wide analysis indicates that yeast pre-mRNA splicing is predominantly posttranscriptional. Mol. Cell *24*, 917–929.

Tseng, C.K., and Cheng, S.C. (2008). Both catalytic steps of nuclear pre-mRNA splicing are reversible. Science *320*, 1782–1784.

Villa, T., Ceradini, F., and Bozzoni, I. (2000). Identification of a novel element required for processing of intron-encoded box C/D small nucleolar RNAs in Saccharomyces cerevisiae. Mol. Cell. Biol. *20*, 1311–1320.

Wahl, M.C., Will, C.L., and Lührmann, R. (2009). The spliceosome: design principles of a dynamic RNP machine. Cell *136*, 701–718.

Xu, Z., Wei, W., Gagneur, J., Perocchi, F., Clauder-Münster, S., Camblong, J., Guffanti, E., Stutz, F., Huber, W., and Steinmetz, L.M. (2009). Bidirectional promoters generate pervasive transcription in yeast. Nature *457*, 1033–1037.